University of Groningen

The ATLAS(3D) project

Martig, Marie; Crocker, Alison F.; Bournaud, Frederic; Emsellem, Eric; Gabor, Jared M.; Alatalo, Katherine; Blitz, Leo; Bois, Maxime; Bureau, Martin; Cappellari, Michele

IMPORTANT NOTE: You are advised to consult the publisher's version (publisher's PDF) if you wish to cite from it. Please check the document version below.

Document Version
Publisher's PDF, also known as Version of record

Link to publication in University of Groningen/UMCG research database

The ATLAS[3D] project – XXII. Low-efficiency star formation in early-type galaxies: hydrodynamic models and observations

Marie Martig,[1]⋆ Alison F. Crocker,[2] Frédéric Bournaud,[3] Eric Emsellem,[4,5]
Jared M. Gabor,[3] Katherine Alatalo,[6] Leo Blitz,[6] Maxime Bois,[7] Martin Bureau,[8]
Michele Cappellari,[8] Roger L. Davies,[8] Timothy A. Davis,[4,8] Avishai Dekel,[9]
P. T. de Zeeuw,[4,10] Pierre-Alain Duc,[3] Jesus Falcón-Barroso,[11,12] Sadegh Khochfar,[13]
Davor Krajnović,[4] Harald Kuntschner,[4] Raffaella Morganti,[14,15]
Richard M. McDermid,[16] Thorsten Naab,[17] Tom Oosterloo,[14,15] Marc Sarzi,[18]
Nicholas Scott,[1] Paolo Serra,[14] Kristen Shapiro Griffin,[19] Romain Teyssier,[3]
Anne-Marie Weijmans[20]† and Lisa M. Young[21]

[1]*Centre for Astrophysics & Supercomputing, Swinburne University of Technology, PO Box 218, Hawthorn, VIC 3122, Australia*
[2]*Department of Astronomy, University of Massachusetts, Amherst, MA 01003, USA*
[3]*Laboratoire AIM Paris-Saclay, CEA/IRFU/SAp CNRS Université Paris Diderot, F-91191 Gif-sur-Yvette Cedex, France*
[4]*European Southern Observatory, Karl-Schwarzschild-Str. 2, D-85748 Garching, Germany*
[5]*Université Lyon 1, Observatoire de Lyon, Centre de Recherche Astrophysique de Lyon and Ecole Normale Supérieure de Lyon, 9 avenue Charles André,
F-69230 Saint-Genis Laval, France*
[6]*Department of Astronomy, Campbell Hall, University of California, Berkeley, CA 94720, USA*
[7]*Observatoire de Paris, LERMA and CNRS, 61 Av. de l'Observatoire, F-75014 Paris, France*
[8]*Sub-department of Astrophysics, Department of Physics, University of Oxford, Denys Wilkinson Building, Keble Road, Oxford OX1 3RH, UK*
[9]*Racah Institute of Physics, The Hebrew University, Jerusalem 91904, Israel*
[10]*Sterrewacht Leiden, Leiden University, Postbus 9513, NL-2300 RA Leiden, the Netherlands*
[11]*Instituto de Astrofisica de Canarias, Vía Láctea s/n, La Laguna, Tenerife, Spain*
[12]*Departamento de Astrofísica, Universidad de La Laguna, E-38205 La Laguna, Tenerife, Spain*
[13]*Max-Planck-Institut für extraterrestrische Physik, PO Box 1312, D-85478 Garching, Germany*
[14]*Netherlands Institute for Radio Astronomy (ASTRON), Postbus 2, NL-7990 AA Dwingeloo, the Netherlands*
[15]*Kapteyn Astronomical Institute, University of Groningen, Postbus 800, NL-9700 AV Groningen, the Netherlands*
[16]*Gemini Observatory, Northern Operations Centre, 670 North A'ohoku Place, Hilo, HI 96720, USA*
[17]*Max-Planck-Institut für Astrophysik, Karl-Schwarzschild-Str. 1, D-85741 Garching, Germany*
[18]*Centre for Astrophysics Research, University of Hertfordshire, Hatfield, Herts AL1 9AB, UK*
[19]*Space Sciences Research Group, Northrop Grumman Aerospace Systems, Redondo Beach, CA 90278, USA*
[20]*Dunlap Institute for Astronomy & Astrophysics, University of Toronto, 50 St. George Street, Toronto, ON M5S 3H4, Canada*
[21]*Physics Department, New Mexico Institute of Mining and Technology, Socorro, NM 87801, USA*

ABSTRACT

We study the global efficiency of star formation in high-resolution hydrodynamical simulations of gas discs embedded in isolated early-type and spiral galaxies. Despite using a universal local law to form stars in the simulations, we find that the early-type galaxies are offset from the spirals on the large-scale Kennicutt relation, and form stars two to five times less efficiently. This offset is in agreement with previous results on morphological quenching: gas discs are more stable against star formation when embedded in early-type galaxies due to the lower disc self-gravity and increased shear. As a result, these gas discs do not fragment into dense clumps and do not reach as high densities as in the spiral galaxies. Even if some molecular gas is present, the fraction of very dense gas (typically above $10^4 \, \mathrm{cm}^{-3}$) is significantly reduced, which explains the overall lower star formation efficiency. We also analyse a sample

⋆ E-mail: marie.martig@gmail.com
† Dunlap Fellow.

of local early-type and spiral galaxies, measuring their CO and H I surface densities and their star formation rates as determined by their non-stellar 8 μm emission. As predicted by the simulations, we find that the early-type galaxies are offset from the Kennicutt relation compared to the spirals, with a twice lower efficiency. Finally, we validate our approach by performing a direct comparison between models and observations. We run a simulation designed to mimic the stellar and gaseous properties of NGC 524, a local lenticular galaxy, and find a gas disc structure and global star formation rate in good agreement with the observations. Morphological quenching thus seems to be a robust mechanism, and is also consistent with other observations of a reduced star formation efficiency in early-type galaxies in the COLD GASS survey. This lower efficiency of star formation is not enough to explain the formation of the whole red sequence, but can contribute to the reddening of some galaxies.

1 INTRODUCTION

At least up to $z \sim 1$, galaxy colours follow a bimodal distribution associated with their stellar morphology, with blue star-forming late-type spiral galaxies (LTGs) and a red sequence of early-type galaxies (ETGs) (e.g. Kauffmann et al. 2003; Cirasuolo et al. 2007). Red ETGs harbour only very low levels of star formation, and although these levels increase with redshift (Tonini et al. 2010), ETGs remain well below the 'main sequence' of star formation (Noeske et al. 2007; Schiminovich et al. 2007; Wuyts et al. 2011; Salmi et al. 2012). The conversion of cold gas reservoirs into stars on the scale of entire galaxies has long been considered to be a universal process independent of the host galaxy properties (e.g. Kennicutt 1998a). In that context, the quenching of star formation in ETGs is in general attributed to the quasi-complete removal and/or heating of cold gas reservoirs, for instance, because of merger-triggered starbursts. However, the residual gas content and late gas infall continue to fuel too high amounts of residual star formation to populate a red sequence, unless extra mechanisms are invoked (Gabor et al. 2011).

Recent observations have actually shown that red ETGs can contain cold gas reservoirs. Massive and extended H I reservoirs are often detected in or around ETGs that are not in clusters (Morganti et al. 2006; Grossi et al. 2009; Thom et al. 2012). In the volume-limited ATLAS³ᴰ sample of nearby ETGs (Cappellari et al. 2011, hereafter Paper I), Serra et al. (2012, hereafter Paper XIII) detect H I in 40 per cent of the galaxies that are not in the Virgo cluster, with H I masses from 10^7 to a few 10^9 M$_\odot$. More relevant for star formation, molecular gas is detected in 22 per cent of ETGs, with an average molecular gas-to-star mass fraction of a few per cent (1–5 per cent, Young et al. 2011, hereafter Paper IV), similar to what is found in some spirals. These molecular gas reservoirs in ETGs are often found in relatively compact discs (Crocker et al. 2011; Davis et al. 2011b, hereafter Paper X), and as a result the typical surface densities of CO-traced molecular gas are not lower in ETGs than in LTGs. Even dense molecular tracers, such as HCN, are now detected in red-sequence ETGs (Krips et al. 2010; Crocker et al. 2012, hereafter Paper XI). The significant mass fraction and relatively high surface density of cold gas in many ETGs make their red optical colours more intriguing, as they should have specific rates of star formation comparable to LTGs containing a few per cent of gas.

However, it has been recently recognized that star formation may be a non-universal process that could depend on the properties of the host galaxies. First, observations have suggested that the efficiency of star formation at fixed gas surface density increases from discs to mergers (Daddi et al. 2010; Genzel et al. 2010). Models explain this increase by the influence of galaxy-scale gravitational interactions on the sub-kpc-scale properties of the interstellar matter (ISM; Teyssier, Chapon & Bournaud 2010; Bournaud et al. 2011). Beyond the striking case of major mergers, there are also more systematic variations of the efficiency of star formation and gas consumption time-scale with host galaxy properties such as colour, stellar mass or stellar mass density (see Saintonge et al. 2011b, 2012, in the COLD GASS sample). The first studies of individual ETGs did not find evidence for departure from the usual Kennicutt relation established for LTGs (Shapiro et al. 2010; Crocker et al. 2011), but there actually seems to be a clear tendency for lower star formation efficiency (SFE) and a longer gas consumption time-scale in galaxies with redder colours, higher stellar mass concentrations, and/or higher stellar mass densities (Saintonge et al. 2011b, 2012).

Theory has a promising explanation for the low SFE in ETGs that did not have their dense cold gas reservoirs entirely removed. The lower total disc self-gravity in the absence of a stellar disc, and the higher shear imposed by stellar spheroids, can make a gaseous disc more stable in an ETG, provided that the gas velocity dispersions remain high enough. This increased disc stability was already noted by Kawata, Cen & Ho (2007) for circumnuclear discs in elliptical galaxies (see also early studies, for instance, Ostriker & Peebles 1973, showing increased disc stability in the presence of a spherical halo).

It was shown by Martig et al. (2009, hereafter M09) in a cosmological zoom-in simulation that the morphological evolution of a galaxy from LTG to ETG can significantly reduce the star formation rate (SFR) in the remaining gas reservoir. This leads to red optical colours in a system that would remain blue if the SFE and gas consumption time-scale were universal and independent of the host galaxy type. This mechanism, dubbed 'morphological quenching' (MQ), has also been noted in zoom-in simulations at redshift $z \approx 2$, where the formation of big star-forming clumps is quenched by bulge growth (Agertz, Teyssier & Moore 2009; Ceverino, Dekel & Bournaud 2010).

In this paper, we present a series of idealized (isolated), high-resolution (5 pc) hydrodynamic simulations of LTGs and ETGs (Section 2). In Section 3, we analyse the variations of the SFE of a given gas disc, depending on the host galaxy type. We confirm that on a Kennicutt diagram ETGs have a SFE up to five times lower than LTGs at fixed gas surface density, consistent with a new

analysis of the cosmological simulations from M09 (in M09 the SFE of the simulated galaxy was not studied). In Section 4, we analyse observations of eight nearby ETGs, for which we measure the CO and H I surface density and star formation using their non-stellar 8 μm emission. We observe an effect quantitatively consistent with our theoretical predictions, namely a SFE lower by a factor of $\sim$2 in ETGs with respect to a control sample of 12 spirals. The agreement between simulations and observations is further tested by a simulation aimed at mimicking the properties of NGC 524, a red ETG in our sample (Section 5). We discuss the robustness of the process and its potential cosmological implications for the growth of the red sequence in Section 6.

2 SIMULATIONS

2.1 Simulation in a cosmological context

MQ is an effect that was first witnessed in a cosmological resimulation presented in M09. In this section, we briefly describe that simulation, but refer the reader to M09 for a detailed description of the simulation technique as well as the time evolution of stellar and gaseous properties for the simulated galaxy.

We use a resimulation technique that consists of first running a dark matter only cosmological simulation, and computing the merger and diffuse matter accretion history for one of the haloes. We then resimulate this history at higher resolution using a particle-mesh code, in which gas dynamics are modelled with a sticky particle scheme. The spatial resolution is 130 pc, and the mass resolution is $1.4 \times 10^5 \, M_\odot$ for stellar particles, $2.1 \times 10^4 \, M_\odot$ for gas particles and $4.4 \times 10^5 \, M_\odot$ for dark matter particles. Star formation is computed with a Schmidt law: the SFR is proportional to the gas density to the exponent 1.5, above a fixed threshold of $0.03 \, M_\odot \, pc^{-3}$. In this simulation, feedback from supernova explosions is not taken into account.

The resimulation is made by replacing each halo of the cosmological simulation by a new model galaxy made of a gas disc, a stellar disc and bulge and a dark matter halo, and by replacing each 'diffuse' dark matter particle with a new group of gas and dark matter particles (mostly corresponding to accretion along filaments). The simulation starts at $z = 2$ and follows the evolution of a galaxy down to $z = 0$, with mergers and gas accretion as prescribed by the initial cosmological simulation.

The halo grows from a mass of $2 \times 10^{11} \, M_\odot$ at $z = 2$ to $1.4 \times 10^{12} \, M_\odot$ at $z = 0$. During that time, the galaxy first undergoes a series of intense minor mergers that transform the initial $z = 2$ disc into a spheroid. From $z \simeq 1.2$ down to $z \simeq 0.2$ is a much quieter phase, dominated by smooth dark matter and gas accretion, with an average gas accretion rate of $9 \, M_\odot \, yr^{-1}$. Finally, a major merger takes place at $z = 0.2$ with a mass ratio of 1.5:1.

During the quiet phase, a gas disc is gradually built within the ETG, with a cold gas mass growing from 5.1×10^9 to $1.3 \times 10^{10} \, M_\odot$. In spite of this large gas content, the SFR remains at a low level, and the galaxy has a red colour. This is the phase corresponding to a MQ effect: the gas disc is stable against star formation because it is embedded in an ETG.

In M09, we discussed the detailed properties of the gas disc, and analysed its stability. In this paper, we will show where the simulated galaxy stands on the Kennicutt relation, and will discuss the SFE as a function of host galaxy morphology.

2.2 Idealized simulations of isolated galaxies

2.2.1 General settings

We perform a series of hydrodynamical simulations with the Adaptive Mesh Refinement (AMR) code RAMSES. The box size is 350 kpc and is covered with a 512^3 grid, corresponding to a minimal level of refinement $l_{\mathrm{min}} = 9$. Additional levels of refinement are added up to $l_{\mathrm{max}} = 16$, so that the maximal spatial resolution is 5.3 pc. A cell is refined if it contains a gas mass greater than $3.7 \times 10^3 \, M_\odot$ or it contains more than 20 particles. This refinement strategy, together with the choice of the pseudo-cooling equation of state, ensures that the Jeans length is resolved by at least four cells at all levels of refinement so that artificial fragmentation is prevented (Truelove et al. 1997). Dark matter particles have a mass of $7500 \, M_\odot$ and stellar particles have a mass of $2500 \, M_\odot$.

The gas is described with a barotropic cooling model (or 'pseudo-cooling'), which has been shown to produce a realistic structure for the simulated ISM (Bournaud et al. 2010). Star formation is modelled with a Schmidt law: when the local gas density exceeds a threshold of $30 \, cm^{-3}$, the local SFR is equal to $\epsilon_* \rho_{\mathrm{gas}}/t_{\mathrm{ff}}$, where t_{ff} is the free-fall time at the density ρ_{gas} and ϵ_* is the efficiency. The efficiency is chosen to be 0.1 per cent and is calibrated so that the simulated spirals follow the observed Kennicutt law (Kennicutt 1998b). The combined choice of a relatively low threshold and a low efficiency is made to remove any possible bias due to some gas clouds being at the resolution limit, especially in the outer disc (where the overall density is lower so that cells are less refined). The size of these cells limits the hierarchy of structures that can collapse, and imposing a low threshold for star formation mimics the fact that some of these cells might have contained subclumps that we do not resolve, and should have formed stars at a low level.

As in Bournaud et al. (2010), supernova feedback is modelled in a kinetic form, where 20 per cent of the energy of supernovae is injected in the gas as a radial kick (the rest of the energy is assumed to be radiated away) within a bubble of radius 20 pc. We use the blast-wave model described in Dubois & Teyssier (2008).

2.2.2 Relaxation of initial conditions

Initially, a galaxy model is not perfectly in equilibrium, but the gas disc needs to reach equilibrium before we start studying its properties. To allow a faster relaxation of initial conditions, we increase the resolution progressively. We start the simulation without star formation, with an isothermal equation of state at $T = 10^4 \, K$ and a maximal resolution of 43 pc corresponding to $l_{\mathrm{max}} = 13$. When a steady state is reached, we turn on the pseudo-cooling, keeping $l_{\mathrm{max}} = 13$. The next steps are to gradually increase the resolution up to $l_{\mathrm{max}} = 16$ so that the full resolution is reached, and to finally turn on star formation and feedback. After this, each of the simulations is run for $\sim$100 Myr.

This method ensures that a steady state is quickly reached, and the SFR is nearly constant for the main part of the simulation (Fig. 1).

2.2.3 Galaxy parameters

We simulate the isolated evolution of four different galaxies, with various Hubble types and gas fractions. Two of these galaxies are elliptical galaxies, with gas fractions of 4.5 and 1.3 per cent (the gas fraction is defined as the ratio of the total gas mass in the disc to the total stellar mass of the galaxy, and includes all gas phases). The
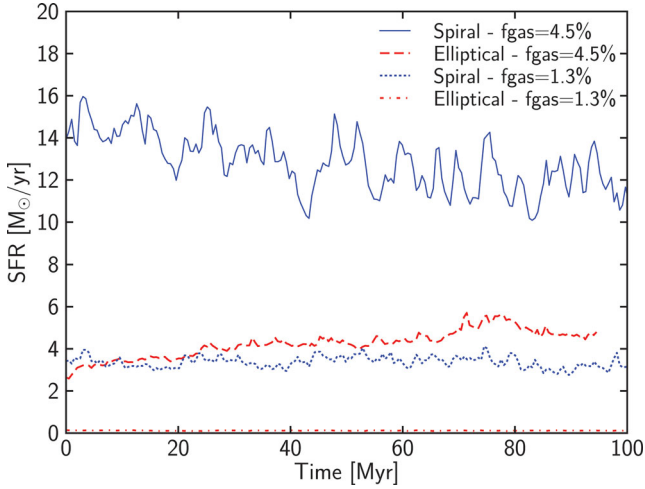
Figure 1. Time evolution of the SFR for the four idealized high-resolution simulations. This shows that the SFR is nearly constant as a function of time, a consequence of a careful relaxation of the initial conditions. The slow decrease with time of the SFR for the spiral with a 4.5 per cent gas fraction is simply due to slow gas consumption. By contrast, the elliptical with a 4.5 per cent gas fraction first goes through a 75 Myr phase of slightly increased gas disc fragmentation and increased SFR, before reaching a steady state.

two others are spirals, with also the same gas fractions of 4.5 and 1.3 per cent.

These gas fractions are chosen because they are representative of the gas content of local ETGs in the ATLAS[3D] sample (Paper IV). In turn, the simulated spirals, which have a stellar mass and size similar to the Milky Way, have a much too low gas fraction to be representative of local spiral galaxies, but serve as a comparison in our study of disc stability.

All galaxies have the same dark matter halo, which has a total mass of $2.5 \times 10^{11} \, M_\odot$ (corresponding to 3.33×10^7 particles), and is modelled with a Burkert profile with a core radius of 14 kpc (Salucci & Burkert 2000). It is truncated at 130 kpc. In all cases, the stellar component has a total mass of $5.6 \times 10^{10} \, M_\odot$ (corresponding to 2.24×10^7 particles). The elliptical galaxies are modelled with a Hernquist profile with a characteristic radius of 1.5 kpc truncated at 40 kpc. The spiral galaxies are made of a $5 \times 10^9 \, M_\odot$ bulge and a $5.1 \times 10^{10} \, M_\odot$ disc so that $B/D = 0.1$. The bulge follows a Plummer profile with a characteristic radius of 1 kpc truncated at 2 kpc and the disc has a Toomre profile with a characteristic radius of 3 kpc truncated at 20 kpc. The gas discs have a mass of 2.5×10^9 and $7.5 \times 10^8 \, M_\odot$ (corresponding to gas fractions of 4.5 and 1.3 per cent, respectively). They follow an exponential profile with a characteristic radius of 1 kpc truncated at 2 kpc. Their velocities are initialized in rotational equilibrium with the whole galaxy, but with no velocity dispersion.

The gas disc parameters (mass and sizes) have been chosen to be within the range of observed values for local ETGs. The average extent of molecular gas in the ATLAS[3D] sample is 1 kpc, with only 15 per cent of gas discs reaching a size of 2 kpc (Davis et al. 2013, hereafter Paper XIV). However, this observed size only concerns molecular gas, which is the most centrally concentrated component, while our simulated discs include all gas phases. In addition, the range of surface densities that the simulations explore (from $\sim$10 to a few $100 \, M_\odot \, pc^{-2}$) is quite typical of the observed densities.

A gas mass of $2.5 \times 10^9 \, M_\odot$ is, however, reached by very few local ETGs, and in that case our choice of disc profile corresponds

to very high central surface densities (a few $100 \, M_\odot \, pc^{-2}$). This represents an upper limit to the gas content of local ETGs, and the other simulated elliptical is probably more representative of the local population. By contrast, the spiral galaxies that we simulate are not representative at all of the local spirals (both in terms of gas fraction and in terms of gas disc radius, which are both too small), but will be useful to perform comparisons with the ellipticals.

3 GAS DYNAMICS AND STAR FORMATION IN SIMULATED GALAXIES

3.1 Star formation efficiency

Hereafter, we define the SFE α as

$$\Sigma_{SFR} = \alpha \times \Sigma_{gas}^\beta, \tag{1}$$

where the star formation surface density Σ_{SFR} is expressed in units of $M_\odot \, yr^{-1} \, kpc^{-2}$ and the gas surface density Σ_{gas} is in $M_\odot \, pc^{-2}$. This definition of the SFE is chosen because it is the easiest one when the exponent β changes from one galaxy to another.

In the left-hand panel of Fig. 2, we show the gas and SFR surface densities in the cosmological simulation studied in M09. We measure these quantities during the MQ phase in five snapshots (500 Myr apart) of the simulation. For each snapshot, average values of Σ_{gas} and Σ_{SFR} are computed within the optical radius of the main galaxy (R_{25} in the g band), and in 10 annuli centred on the centre of the galaxy (each annulus has a width of 1 kpc, and the galaxy is taken face-on). The same method is applied to other snapshots of the same simulation, when the galaxy is actually a star-forming disc at $z \sim 2$ before the first minor mergers occur, and at $z \sim 0$.

Except at very low gas density, the star-forming discs lie within 1σ of the best fit proposed by Kennicutt (1998b). The red ETGs undergoing MQ roughly occupy the same region of the Kennicutt plot as the star-forming discs, although very high gas densities are not found in the MQ phase. As expected, on average the quenched gas discs tend to lie slightly below the star-forming galaxies (i.e. to have a lower Σ_{SFR} for a given Σ_{gas}). We fit the efficiency and slope of the Kennicutt relation (equation 1) for each series of points independently, not taking into account the points at low gas density and low SFR that would artificially skew the slope to a too high value (and might be affected by our choice of threshold for forming stars in the simulation). We list in Table 1 the best-fitting values for the efficiency and slope of the Kennicutt relation. The efficiency and slope for the spiral galaxies are very close to the best-fitting values proposed by Kennicutt (1998b), while the ETG has much lower efficiency but also a much steeper slope. This steep slope makes it hard to compare the efficiency directly with the one found for the spirals. To help with the interpretation of the results, we draw a line in Fig. 2 with the same slope as the spirals' one and that goes through the points corresponding to global averages. This line gives an efficiency of star formation 2.5 times lower in the ETG compared to the spirals. We test if this result still holds in the 5 pc resolution simulations of gas discs embedded in an idealized spiral or elliptical galaxy. We now measure the gas and SFR surface densities within 500 pc wide annuli between 0 and 2 kpc from the centre of the galaxy (see the right-hand panel of Fig. 2). This amounts to four data points per simulated galaxy, except for the spiral with the lowest gas mass: in that galaxy, the outer regions have a very low gas density and do not host any star formation, so that only the first two radial bins are considered.

We fit both simulated spirals with the same slope and efficiency. We perform separate fits for the two elliptical galaxies since they
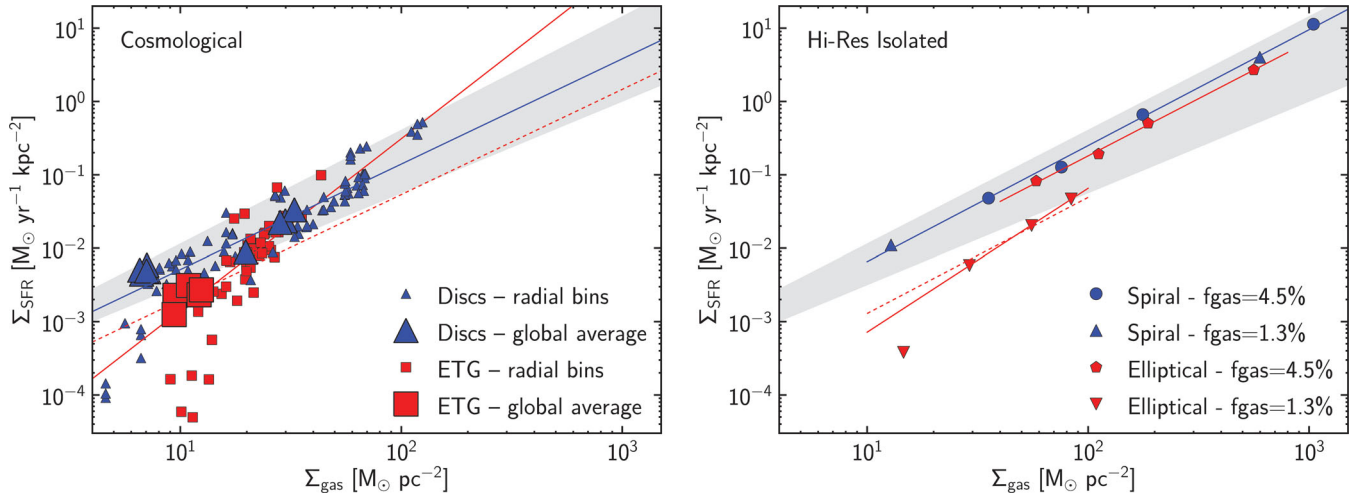
Figure 2. Simulated ETGs and spirals on the Kennicutt relation. Left-hand panel: for a cosmological resimulation. Right-hand panel: for idealized simulations with a maximal resolution of 5 pc. In both cases, the shaded area is the 1σ zone from Kennicutt (1998) and the solid lines are fits to the simulated data points (for the idealized ellipticals, a fit is performed separately for the two galaxies since they have very different behaviours). The dashed red lines are there to guide the eye and are simply the fits for the spiral population but with an efficiency divided by 2.5 (left-hand panel) or 5 (right-hand panel).

Table 1. Best-fitting values for the efficiency and slope of the Kennicutt relation for simulated galaxies.

Simulation	Efficiency	Slope
Cosmological		
Disc	1.9×10^{-4}	1.4
Early type	6.5×10^{-6}	2.3
Idealized		
Spirals	1.7×10^{-4}	1.6
Elliptical, $f_g = 4.5$ per cent	1.4×10^{-4}	1.6
Elliptical, $f_g = 1.3$ per cent	7.9×10^{-6}	2.0

have a very different behaviour (see the resulting best-fitting values in Table 1). The elliptical with a large gas fraction (and thus a high gas surface density) lies very close to the spirals' best fit : the slope is the same in both cases, and the SFE is only 1.2 times lower. By contrast, the elliptical galaxy with a lower gas content is clearly offset from the relation followed by the spirals, and has a lower SFE. As for the elliptical in the cosmological simulation, the slope of the Kennicutt relation is also steeper for this galaxy. Drawing a line passing through the data points but with the same slope as for the spirals gives a factor of 5 difference between the SFE in this elliptical compared to the spirals.

We thus do not predict that ETGs are completely off the relation observed for spirals, but that they have a SFE up to a factor of 5 lower than spirals. The amount by which the efficiency is reduced depends strongly on the gas disc properties, which we will study next.

3.2 Gas disc properties

To better understand the difference in SFE as a function of the host galaxy morphology, we study the properties of the gas discs in the four generic simulations. The top panels in Fig. 3 show the gas surface density maps after 100 Myr of evolution at full resolution. We also show the gas density profiles and the gas density probability distribution functions (PDFs) in Fig. 4. While all simulations started with a smooth exponential gas disc, we find that the subsequent

evolution depends strongly both on the total gas content (more precisely on the gas surface density) and on the Hubble type of the host galaxy, in agreement with our previous results on MQ.

For a relatively low surface density and gas fraction, we find that the gas disc is extremely stable when embedded in the elliptical galaxy. It keeps an exponential profile with a similar scalelength to the initial disc, and does not fragment into dense clumps, although some small spiral armlets can be seen in Fig. 3. The gas densities do not reach values greater than 10^3 cm^{-3}, and only 26 per cent of the gas mass is found at densities greater than 10^2 cm^{-3} (a typical value for molecular gas formation). As a consequence, the SFR remains very low, at only $0.1\,\mathrm{M_\odot}$ yr^{-1}. Note that the gas disc is stable in spite of a very low turbulent velocity dispersion (Table 2 and bottom left-hand panel of Fig. 3). The low velocity dispersion is the consequence of both the gravitational stability and very few supernova explosions. Some of the gas disc stability is probably provided by the thermal velocity dispersion.

By contrast, we find that a spiral galaxy with a similar initial gas content has very different behaviour. The gas disc is heavily fragmented, and the migration of the gas clumps under the effect of dynamical friction concentrates the gas towards the centre of the galaxy so that the final density profile is strongly changed (Figs 3 and 4). Within these clumps, the gas can reach densities of a few 10^5 cm^{-3} (see the PDF in Fig. 4). In contrast to the case of the elliptical galaxy, 89 per cent of the gas mass is found at densities greater than 10^2 cm^{-3}, and 51 per cent of the mass reaches densities typical of prestellar cores (10^4 cm^{-3}). The spiral galaxy then forms stars at an average rate of $3.8\,\mathrm{M_\odot}$ yr^{-1}, a rate nearly a factor of 40 greater than in the elliptical galaxy.

The differences between the spiral and elliptical are not so pronounced at high gas surface densities. We find that in the elliptical with a 4.5 per cent gas fraction, the disc is not stable against fragmentation into clumps (see Fig. 3). Both the surface density map and profile are rather similar for the spiral and the elliptical. However, some differences can still be seen in the gas density PDFs, with a PDF shifted to higher densities in the spiral galaxy. Indeed, while the spiral and the elliptical have a similar fraction of their gas in molecular form (72 per cent in the elliptical versus 87 per cent in the spiral), the fraction of very dense ($>10^4$ cm^{-3}) gas is 2.4 times

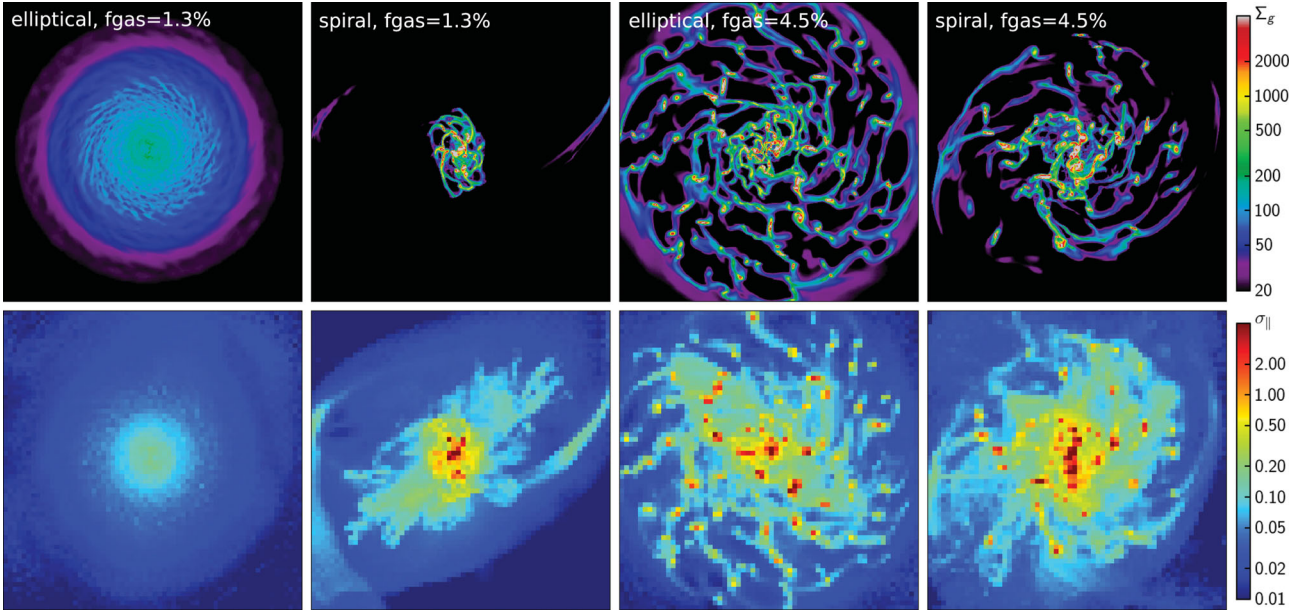**Figure 3.** Face-on maps of the gas surface density and velocity dispersion. The top panels show the gas surface density (5×5 kpc panels, colour map in units of $M_\odot$ pc^{-2}) for the four generic simulations. The bottom panels show the corresponding in-plane velocity dispersion $\sigma_\parallel = \sqrt{\sigma_x^2 + \sigma_y^2}$, mass averaged along the line of sight, computed in 80×80 pc pixels (5×5 kpc panels, colour map in units of km s^{-1}).
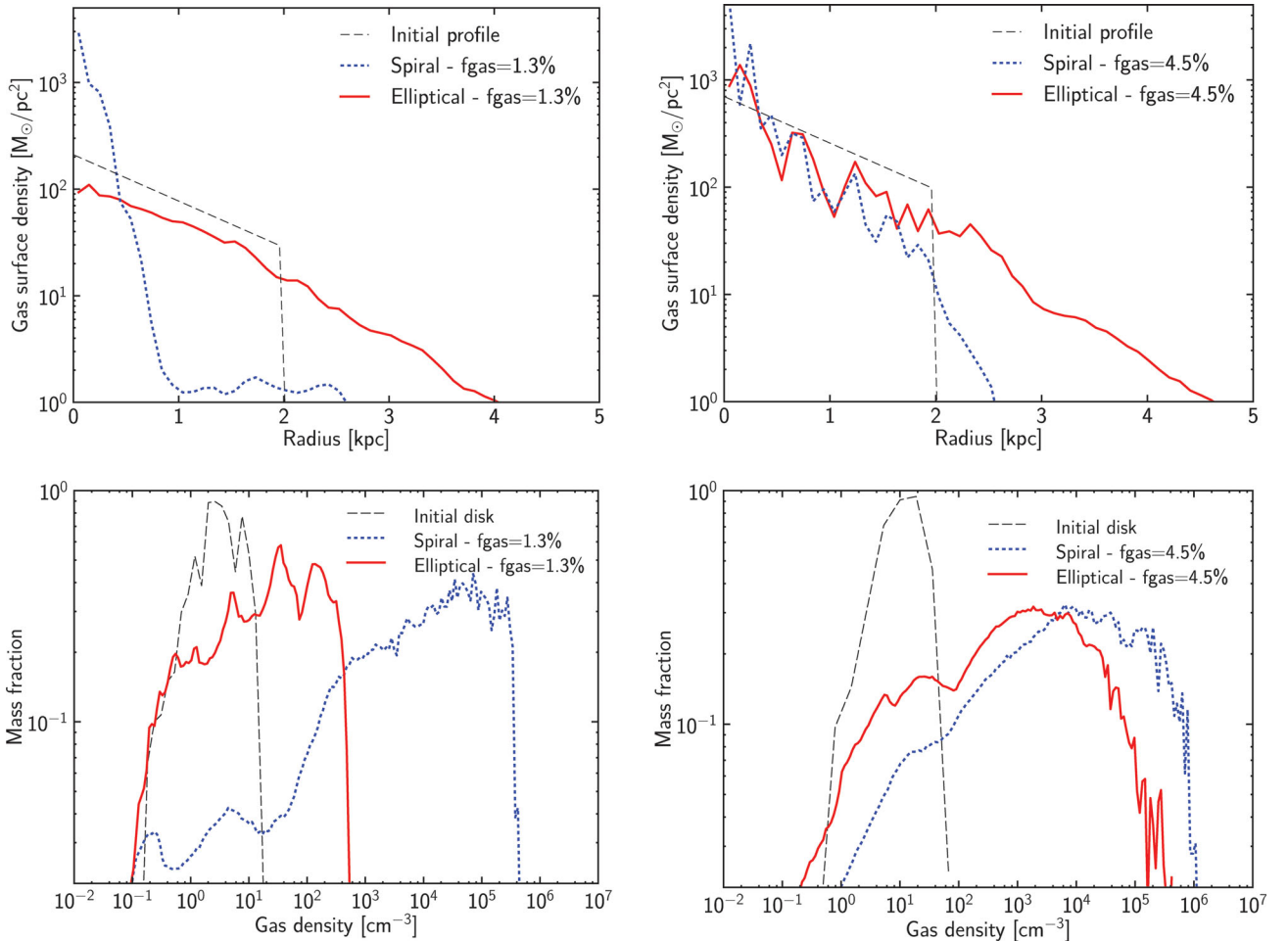

Figure 4. Gas surface density profiles (top panels) and gas density PDFs (bottom panels) for the spiral and elliptical with a gas fraction of 1.3 per cent (left-hand panels) and 4.5 per cent (right-hand panels). In each case, the initial profile is also shown.

Table 2. Gas disc properties and SFR (averaged over the last 5 Myr of the simulations) for the four idealized simulations.

Simulation	$\sigma_\perp$ (km s^{-1})	$\sigma_\parallel$ (km s^{-1})	f_g ($>10^2$ cm^{-3})	f_g ($>10^4$ cm^{-3})	M_g ($>10^4$ cm^{-3}) (M$_\odot$)	SFR (M$_\odot$ yr^{-1})
Elliptical $-f_g = 1.3$ per cent	0.02	0.04	0.26	0.00	0.0	0.1
Spiral $-f_g = 1.3$ per cent	2.48	5.22	0.89	0.51	3.8×10^8	3.8
Elliptical $-f_g = 4.5$ per cent	1.05	1.74	0.72	0.18	4.5×10^8	4.7
Spiral $-f_g = 4.5$ per cent	2.97	5.26	0.87	0.43	10.7×10^8	11.3

higher in the spiral, resulting in a SFR 2.4 times higher than in the elliptical.

In the idealized simulations, the SFR is actually directly proportional to the mass of gas at densities greater than 10^4 cm^{-3} (see the last two columns of Table 2), except in the elliptical with the smallest gas fraction. In that case, there is some residual star formation (at 0.1 M$_\odot$ yr^{-1}) in spite of no gas at high densities; this is because of the very low density threshold (30 cm^{-3}) we used for star formation in all simulations.

The effect of MQ is thus to change the shape of the gas density PDF in ETGs, and to change their fraction of dense gas. Given that we assume a star formation law which is universal on local scales, the smaller amounts of dense gas naturally translate into lower levels of star formation in ETGs. We will discuss this further in Section 6.2, but we will first study if such a MQ effect can also be observed in local ETGs.

4 RESOLVED OBSERVATIONS OF MOLECULAR GAS AND STAR FORMATION IN EARLY-TYPE GALAXIES

To compare our simulations to observed galaxies, we select eight galaxies from the ATLAS^{3D} sample of ETGs. All eight have molecular gas maps based on interferometric ^{12}CO(1–0) data, atomic gas maps and SFR maps obtained using the 8 μm polycyclic aromatic hydrocarbon (PAH) band as a SFR indicator. This sample is made of all galaxies for which this information is available, after removing one galaxy (NGC 3489). NGC 3489 has a very unusual molecular gas distribution, including spiral arms. This suggests that the gas is gravitationally unstable, and is consistent with NGC 3489 being a flat, discy galaxy, with stars that might contribute to the disc instability. In addition, the molecular gas has an irregular velocity field suggesting that it has been recently accreted or disturbed (Crocker et al. 2011). Because of these uncertainties, we exclude this galaxy from the sample. Details of the sample galaxies are listed in Table 3.

For comparison, we analyse a sample of 12 LTGs: NGC 628, 2903, 3351, 3521, 3627, 4736, 4826, 5055, 5194, 5457, 6946 and 7331. This sample consists of all LTGs with available CO from BIMA-SONG (selecting only those with both Berkeley Illinois Maryland Array (BIMA) and 12-m observations, Helfer et al. 2003), H I from THINGS (Walter et al. 2008) and 8 μm data from SINGS (Kennicutt et al. 2003) or LVL (Dale et al. 2009). These galaxies are at similar distances (5–15 Mpc) to our ETG sample galaxies.

4.1 Observational gas surface densities

Gas surface densities are derived using CO and H I interferometric observations. We use the ^{12}CO(1–0) transition as a tracer of molecular gas, using a conversion factor of $X_{CO} = 3 \times 10^{20}$ cm^{-2} (K km s^{-1})$^{-1}$. Half of the ETG CO maps (NGC 3032, 4150, 4459 and 4526) were obtained using BIMA with details of observational setup and data reduction in Young, Bureau & Cappellari (2008). The other half of the CO maps (NGC 524, 2768, 4477 and 4550)

Table 3. The sample of observed ETGs.

Name	Distance (Mpc)	H$_2$ mass log (M$_\odot$)	H I mass log (M$_\odot$)	$f_{3.6}$	PA	Axial ratio
NGC 524	23.3	7.8	<6.4	0.293	36.5	1.06
NGC 2768	21.8	7.8	7.8	0.258	180	1.20
NGC 3032	21.4	8.7	7.8	0.293	92.5	2.06
NGC 4150	13.4	7.7	6.0	0.264	146	1.44
NGC 4459	16.1	8.2	<6.6	0.264	89	1.47
NGC 4477	16.5	7.4	<7.0	0.261	227	1.20
NGC 4526	16.4	8.8	<7.9	0.268	108	2.28
NGC 4550	15.5	6.9	<6.5	0.268	179	3.55

Notes. Distances from Paper I. H$_2$ masses from Crocker et al. (2011) and use $X_{CO} = 3 \times 10^{20}$ cm^{-2} (K km s^{-1})$^{-1}$. H I masses from Paper XIII or Crocker et al. (2011). $f_{3.6}$ is the multiplicative factor applied to the IRAC 3.6 μm image when it is subtracted off the 8 μm image in order to remove the stellar emission at 8 μm (Shapiro et al. 2010). PAs are from Cappellari et al. (2007) and axial ratios are derived from best inclinations from Davis et al. (2011a, Paper V).

were obtained with the Plateau de Bure Interferometer (PdBI) with details in Crocker et al. (2008), Crocker et al. (2009) and Crocker et al. (2011).

Our choice of X_{CO} is based upon the typical value for Milky Way clouds. It is known that X_{CO} varies based upon metallicity, reaching much higher values in low-metallicity systems (e.g. Wilson 1995; Arimoto, Sofue & Tsujimoto 1996). Meanwhile, highly active galaxies such as starbursts and ultraluminous infrared galaxies have lower values of X_{CO} (e.g. Wild et al. 1992; Solomon et al. 1997). Unfortunately, little is yet known about what the appropriate value for ETGs may be. Recent theoretical modelling suggests that X_{CO} is not a function of galaxy morphology, depending most strongly on metallicity and more weakly upon radiation field and column density (Feldmann, Gnedin & Kravtsov 2012; Narayanan et al. 2012). None of the ETGs chosen for this work is a starburst and furthermore many have low [O III]/Hβ ratios signalling relatively high gas-phase metallicities. Therefore, a choice of $X_{CO} = 3 \times 10^{20}$ cm^{-2} (K km s^{-1})$^{-1}$ is at least plausible for the ETG sample and simplifies the comparison with the spiral galaxies, for which we will use the same value of X_{CO}.

We sum the flux density in the CO maps of these galaxies within annular ellipses. The annuli are centred at each galaxy's optical centre with widths equal to the average of the interferometric beam major and minor axes in order to keep the measurements independent. The position angle (PA) and axial ratio of the ellipses are listed in Table 3. No background subtraction is performed for the CO photometry.

The H I data obtained with the Westerbork Synthesis Radio Telescope are less well resolved (beams typically >30 arcsec) and so we only have 'central' values of H I mass (Paper XIII). We assume this mass is uniformly distributed over the observed CO distribution. While the H I/H$_2$ ratio almost certainly varies within each galaxy, we note that the inclusion of H I is always a minor consideration for

the ETGs, as they have only ≈10 per cent or less of their cold gas mass in H I in these regions.

An identical approach is followed for the LTGs, including using the same X_{CO} factor. The only change is the use of the interferometric H I maps from the VLA as obtained by the THINGS project. The resolution of these maps is ≈6 arcsec, so we are able to use the H I map itself, combined with the CO maps to obtain a total cold gas surface density.

The dominant error in the gas surface density is the calibration uncertainty associated with the CO observations, taken to be 20 per cent. We also add in quadrature a component for the estimated photometric error, based upon the noise level in the original data cubes.

4.2 Observational SFR surface densities

For both ETGs and LTGs, we compute SFRs using their non-stellar 8 μm emission. Emission from this wavelength predominantly traces band emission from PAHs. We choose 8 μm as a SFR indicator because its resolution is better than some other available indicators [2.82 arcsec compared to: *GALEX* FUV (far-ultraviolet) at 4.5 arcsec, *Spitzer* 24 μm at 6.4 arcsec]. We note that Hα would have a better resolution than 8 μm, but too few (two) of our ETGs have available Hα maps. To obtain a measure of the non-stellar 8 μm emission, we subtract a fraction of the 3.6 μm IRAC band ($f_{3.6}$; dominated by stellar continuum) from the 8 μm IRAC band. The fraction used changes from galaxy to galaxy and is based on stellar population models as in Shapiro et al. (2010). These values are listed for the ETGs in Table 3 and a constant fraction of 0.293 is used for the LTGs.

Photometry is performed in the same elliptical annuli as used for the gas. Background subtraction is performed before the stellar subtraction in both the 3.6 and 8 μm images, and the recommended aperture corrections are applied.

For the conversion to SFR, we turn to the papers of Wu et al. (2005a) and Zhu et al. (2008) which give SFR conversions for the IRAC 8 μm band based upon comparisons to other SFR tracers [radio, Hα, IR (infrared), UV]. We convert these from a Salpeter to Kroupa initial mass function (IMF) and find conversion factors from 1.06×10^{-43} to 1.303×10^{-43} (converting from luminosity in erg s^{-1} to SFR in M$_\odot$ yr^{-1}), based on the tracers used for comparison. We opt to take a rough average conversion factor of 1.2×10^{-43} in this work. We note that some fraction of the 8 μm emission will be contributed by old stars exciting PAH molecules and not exclusively UV photons from young star-forming regions (Crocker et al. 2013). Due to the concentration of old stars in the bulges of ETGs (where the molecular gas is also found), the ETGs likely have a larger contribution to their 8 μm emission from old star heating (Xilouris et al. 2004; Kaneda et al. 2008). However, the 8 μm emission is well tied to the hot dust emission in the 24 μm band in ETGs (Crocker et al. 2011). Thus, the 8 μm SFRs are not likely to be far off, but should be strictly regarded as upper limits for the ETGs.

The error for the derived SFRs includes the photometric error, a 3 per cent error from IRAC calibration in both the 3.6 and 8 μm images and a systematic error of 10 per cent on the stellar subtraction fraction. These are combined in quadrature.

4.3 Results

Our derived gas and star formation surface densities are listed in Table 4 for the ETGs. In Fig. 5, we plot the values for both the ETGs and the LTGs. While there is some spread in both populations, the points corresponding to the annular averages for ETGs are biased

Table 4. Observational results for ETGs.

| Radius (kpc)	Σ_{gas} (M$_\odot$ pc^{-2})	Σ_{SFR} (M$_\odot$ yr^{-1} kpc^{-2})
NGC 524		
0.31	77.9 ± 16.3	0.0373 ± 0.0051
0.62	32.8 ± 6.6	0.0195 ± 0.0024
0.92	11.4 ± 2.3	0.0084 ± 0.0013
NGC 2768		
0.18	47.4 ± 9.5	0.0173 ± 0.0038
NGC 3032		
0.58	204.1 ± 39.6	0.1029 ± 0.0032
1.15	81.3 ± 15.1	0.0218 ± 0.0007
1.73	20.4 ± 3.5	0.0037 ± 0.0001
NGC 4150		
0.44	77.1 ± 15.7	0.0380 ± 0.0017
0.89	7.2 ± 1.5	0.0035 ± 0.0002
NGC 4459		
0.57	119.1 ± 23.9	0.0632 ± 0.0034
1.14	17.3 ± 3.5	0.0051 ± 0.0007
NGC 4477		
0.22	114.5 ± 23.0	0.0141 ± 0.0045
NGC 4526		
0.35	637.4 ± 127.6	0.2037 ± 0.0095
0.70	265.3 ± 53.1	0.0705 ± 0.0033
1.05	45.7 ± 9.2	0.0094 ± 0.0012
NGC 4550		
0.33	15.5 ± 3.2	0.0081 ± 0.0017
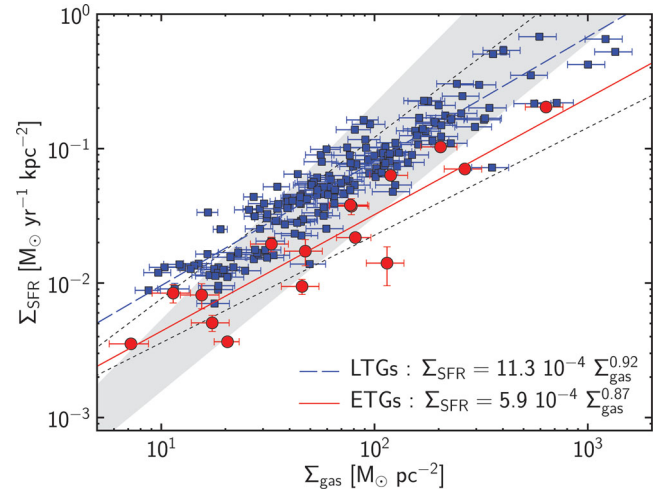
Figure 5. SFR and total gas surface densities for a sample of local LTGs (blue squares) and ETGs (red dots). For each galaxy, these values are computed in several radial bins depending on the extent of the molecular gas. We also show the 1σ zones from Kennicutt (1998) (shaded area) and Bigiel et al. (2008) (dotted lines), both corrected for our X_{CO} value and for a Kroupa IMF. The solid blue and red lines are fits to the data points, showing an average SFE lower by a factor of ~2 in ETGs.

towards having lower values of Σ_{SFR} at a given gas surface density. We note that this is an improvement on earlier works (Shapiro et al. 2010; Crocker et al. 2011) that were unable to distinguish an ETG offset. We now spatially resolve the gas and star formation and we also gain diagnostic power by directly treating spiral galaxies with an identical methodology. Additionally, as noted above, we

excluded a galaxy with an irregular molecular gas distribution, which the previous studies had included.

We fit each population separately, and find that the fits for ETGs and LTGs show a similar slope, which is close to linear as previously found for LTG samples (e.g. Bigiel et al. 2008). However, the efficiency of star formation is lower by a factor of ∼2 in the ETGs, and all ETG data points are below the best-fitting line for the LTGs. This lower efficiency of star formation is consistent with MQ and the findings from the simulations.

5 A DETAILED STUDY OF NGC 524

In our series of idealized simulations, we studied gas discs in perfectly spherical, non-rotating elliptical galaxies. However, in the local Universe such galaxies are very rare, and rarely contain molecular gas (Paper IV): most ETGs containing molecular gas are fast rotators. To understand if MQ is still efficient in a more realistic galaxy with a stellar disc component, and to test the agreement between observations and simulations, we have also performed a RAMSES simulation dedicated to the study of one of our sample ETGs: NGC 524.

NGC 524 is a red lenticular galaxy (a fast rotator) seen close to face-on, it has a central disc containing 6.7×10^7 M$_\odot$ of molecular gas within a radius of 1.1 kpc (Crocker et al. 2011), and an estimated SFR of 0.035–0.051 M$_\odot$ yr^{-1}. NGC 524 was chosen for this comparison because of the regular, symmetric structure of its gaseous and stellar components (with also regular kinematics), suggesting the absence of recent accretion events. It also hosts a well-resolved dust disc, the structure of which we can compare to simulations.

5.1 Simulation setup

The initial conditions for the simulation of NGC 524 have been derived based on an individual multi-Gaussian expansion (MGE) model (Emsellem, Monnet & Bacon 1994) in the course of the ATLAS^{3D} project (Scott et al. 2012).

The MGE model is fitted to ground-based images with the IDL fitting implementation from Cappellari (2002): the stellar component is defined as a sum of two-dimensional Gaussians which are then deprojected to three-dimensional Gaussians using an inclination of $19°$ for NGC 524. We find a total stellar mass of 4.3×10^{11} M$_\odot$. The gas and dark matter components are finally added using an MGE representation of an exponential disc and a Burkert profile, respectively. The dark matter halo has a core radius of 15 kpc (corresponding to $3R_e$), and its mass is 1.6×10^{13} M$_\odot$ so that dark matter represents one-third of the total mass within $3R_e$.

The full model (stars, gas, dark matter) is then used to generate initial conditions using the PYTHON PYMGE module (Emsellem et al., in preparation). The PYMGE package takes the MGE models and solves Jeans equations directly, assuming a cylindrically oriented velocity ellipsoid, while allowing for general axial ratios of the ellipsoid and concatenation of Gaussian components. This is done with the efficient MGE formalism of Emsellem et al. (1994), with the general axial ratio case as in Cappellari (2008), and grouping of Gaussians as described in Emsellem et al. (in preparation). We thus derive a model including the positions and velocities for 2.1 million particles (10^6 for the stars, 10^6 for the halo, and 10^5 for the gas) consistent with the specified underlying MGE mass distribution. Note that the gas component is replaced when feeding these models in the RAMSES code to make it consistent with the AMR scheme. However, the gas itself is included during the generation of the

initial conditions to make sure we obtain a fully self-consistent dynamical realization.

In the RAMSES simulation, the gas disc initially has a mass of 1.6×10^8 M$_\odot$, with an exponential scalelength of 480 pc. It is initially truncated at 2.4 kpc. For this simulation, the refinement strategy, cooling model, star formation and feedback parameters are the same as for the generic idealized simulations.

5.2 A comparison of gas disc properties and star formation rate

We show in Fig. 6 a comparison of the simulated gas disc morphology with a map of the CO emission obtained with PdBI and with an *F555W* unsharp-masked image from the *Hubble Space Telescope* Wide-Field Planetary Camera 2, showing tightly wound spirals of optically obscuring dust. This tightly wound spiral structure is also found in the simulated gas disc, which has a flocculent structure with many small spiral armlets. The small pitch angle is consistent with the galaxy having a massive bulge, and thus a high shear rate (Julian & Toomre 1966; Grand, Kawata & Cropper 2012).

The total SFR is also similar in both cases, with a simulated value of ∼0.045 M$_\odot$ yr^{-1}, while the observed SFR is in the range 0.035–0.051 M$_\odot$ yr^{-1}. This low value is consistent with the simulated gas density PDF, which is typical of a stable gas disc, with a maximal density of 5×10^3 cm^{-3}.

The star formation and gas surface densities are computed for the simulation in the same radial bins as for the observation, and the result is shown in Fig. 7. We see an offset between observation and simulation in this Kennicutt plot, mostly because the simulation does not reproduce the observed gas density profile, which is much flatter. However, both highest density points are a good match. Note that some differences between model and observation may also arise because NGC 524 is seen close to face-on, which makes the mass deprojection very degenerate (Lablanche et al. 2012, hereafter Paper XII).

However, no simulation parameter was tuned to reproduce the observed SFR: the parameters are kept the same as for the generic simulations, including the SFE (that was initially adjusted to reproduce the position of disc galaxies on the Kennicutt relation). The
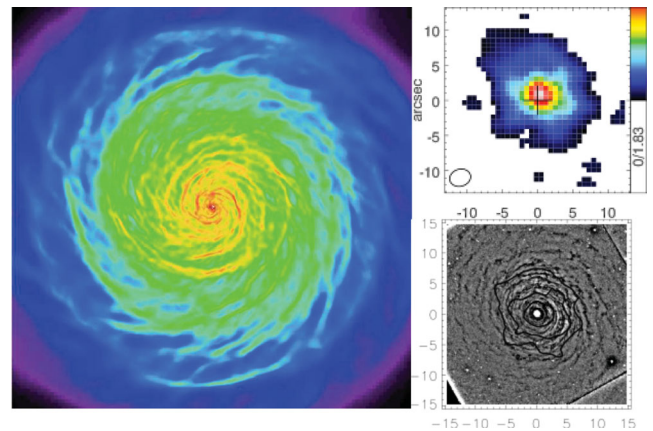

Figure 6. Gas distribution in NGC 524. Left-hand panel: simulated face-on gas surface density map (4×4 kpc). Right-hand panels: integrated intensity map of CO(1–0) (Jy beam^{-1} km s^{-1}), revealing the distribution of cold gas in NGC 524 (top), and unsharp-masked *HST* WFPC2 *F555W* image showing optically obscuring dust, with CO(1–0) contours overlaid in black (bottom). A similar morphology is found in the model and the data, with a tightly wound spiral structure in both cases.
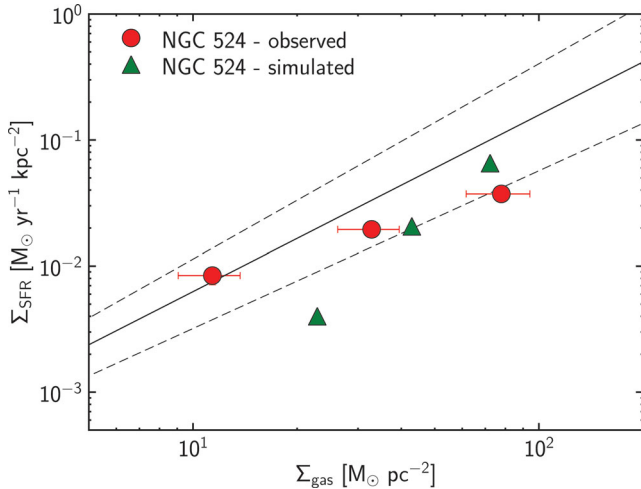
Figure 7. A comparison of observed and simulated star formation and gas surface densities for NGC 524, computed in three radial bins with outer radii of 0.3, 0.6 and 0.9 kpc. The solid line represents the Kennicutt (1998) best fit and the dashed lines show the 1σ range. The gas density profiles do not match, with a much steeper profile in the simulated galaxy. However, the overall decrease of the SFE in the simulation is consistent with the observed value, and the total SFRs are very close.

good match we obtain is reassuring both from the numerical and observational sides.

6 DISCUSSION

6.1 Robustness of the MQ mechanism

We witnessed and studied MQ in different types of simulations, from low-resolution cosmological zoom-ins to high-resolution idealized galaxies. In addition to having different resolutions, these simulations were performed with different gas modelling techniques and different implementations of subgrid recipes for star formation and feedback. We also note that while the idealized case assumes a perfectly spherical galaxy, both the cosmological simulation and the simulation of NGC 524 (a lenticular galaxy) reproduced more realistic mass distributions. MQ is thus effective as long as galaxies are bulge dominated, and not only in perfectly spherical galaxies.

Finally, MQ has also been observed in simulations by other groups, in particular by Agertz et al. (2009) and Ceverino et al. (2010) for high-redshift galaxies (see also a theoretical discussion in Dekel, Sari & Ceverino 2009). This means that from a simulation point of view, this is a robust mechanism, with now several different simulations showing a reduced SFE in ETGs.

From the observational point of view, several factors could influence the position of our sample on the Kennicutt relation. The offset between ETGs and spirals could in theory arise from a different conversion of CO luminosity into mass of molecular gas for these two galaxy types. However, removing the offset would require the ETGs to have a lower X_{CO} than spirals, which is inconsistent with their higher metallicities. There is also some uncertainty on the derivation of the SFR from the non-stellar 8 μm emission, but the choices we made should be conservative (see Section 4), and provide upper limits to the positions of our ETGs on the Kennicutt relation.

Some final uncertainties concern the IMF in the quenched gas discs in the ETGs. Previous studies found that the ongoing star formation events in more massive and denser galaxies have a more top-heavy IMF than Salpeter. They used indirect methods relating galaxy colours or UV fluxes to the Hα ionized gas emission (Hoversten & Glazebrook 2008; Meurer et al. 2009; Gunawardhana et al. 2011). More direct indication of the non-universality of the IMF in galaxies comes from the analysis of IMF-sensitive spectral absorption features. These indicate a bottom-heavy IMF in massive ellipticals (van Dokkum & Conroy 2010). The dynamical modelling of the ATLAS^{3D} sample found a systematic variation in the mass normalization of the IMF within the ETG population. This varies from Kroupa/Chabrier to Salpeter or heavier, as a function of the galaxy density or velocity dispersion (Cappellari et al. 2012a,b, hereafter Paper XX). The spectral and dynamical analyses measure the integrated IMF over the past history of the galaxy and not the present-day IMF that is relevant for this study. However, all these results together indicate that the IMF varies systematically with galaxy properties and possibly with time. If less high-mass stars, or more low-mass ones, are formed in the present-day ETGs with respect to spirals, the same luminosity would correspond to a higher mass of stars formed, and we would thus underestimate the SFR in ETGs (for instance, by a factor of 1.44 if ETGs had a present-day IMF closer to Salpeter than to Kroupa).

The relatively good agreement between simulation and observation of NGC 524 gives us confidence that the reduced SFE in ETGs is real and not an artefact of the handling of the observations, or of the way simulations are performed. In addition, a body of other observational evidence of MQ in nearby galaxies is now published, and we will discuss them in Section 6.3.

6.2 From a universal local SFE to global variations as a function of the host galaxy

Assuming a universal conversion of dense gas into stars, our simulations reproduce variations of the global SFE. Assuming that the small-scale efficiency is universal seems reasonable based both on theoretical and on observational grounds. A universal conversion of dense gas into stars is suggested by the observed linear correlation between SFR and mass of dense molecular gas (as measured by the HCN luminosity) both in the Milky Way and other galaxies (Gao & Solomon 2004; Wu et al. 2005b; Lada et al. 2012). The global SFE then only depends on the fraction of molecular gas in a dense phase, with, for instance, starburst galaxies having higher HCN/CO ratios (Gao & Solomon 2004). These observations can be interpreted by assuming a simple local law, considering the dense clumps within giant molecular clouds as the standard units for star formation, with properties that do not change as a function of environment (Wu et al. 2005b; Krumholz & Thompson 2007; Krumholz, Dekel & McKee 2012).

Instead, what changes from one galaxy to another is the amount of gas in these dense clumps, and their spatial distribution. For instance, in galaxy mergers, the global efficiency of star formation seems higher (Daddi et al. 2010; Genzel et al. 2010), and simulations by Teyssier et al. (2010) show that this can be explained by a universal local law but a gas density PDF skewed towards very high densities, with gas fragmented into very dense clumps. Variations in the shape of the PDF have similarly been used by Renaud, Kraljic & Bournaud (2012) to explain variations in global SFE from dwarf galaxies to high-redshift mergers.

MQ results from a similar effect. In ETGs the gravitational stability of gas discs is enhanced, and their density PDF is skewed towards lower densities. In some cases, they do not even reach the densities that would be typical of dense clumps (for instance, gas

that would be traced by HCN). In ETGs, the simulations thus predict a lower dense gas fraction than in spirals, which has tentatively been observed for a small sample in Paper XI. Given the shapes of the simulated PDFs, the HCN-to-H I ratio should also be lower in ETGs than in spirals.

If the picture of a universal local efficiency is true, then we also predict that ETGs should follow the same linear correlation between SFR and HCN luminosity as spiral galaxies, which has been observed by Krips et al. (2010) for three SAURON ETGs but would require a larger sample to be definitely confirmed.

6.3 Other possible evidence of MQ in the local Universe

Numerous photometric studies, both at low and high redshift, have shown that galaxies with lower levels of star formation tend to have a higher Sérsic index, a higher stellar mass surface density (or 'inferred' velocity dispersion) and to be more concentrated than star-forming galaxies (e.g. Kauffmann et al. 2003; Bell 2008; Franx et al. 2008; Williams et al. 2010; Wuyts et al. 2011; Bell et al. 2012). Combining the Fundamental Plane of ETGs with stellar population information, Graves, Faber & Schiavon (2009) found that indeed the actual velocity dispersion is a better predictor of a galaxy's past star formation history than the galaxy stellar mass. The ATLAS[3D] project, thanks to accurate and unbiased masses from the dynamical modelling of the sample, confirmed that no other dynamical parameter predicts ETG properties better than velocity dispersion (Cappellari 2011b; Paper XX). The same conclusion was reached by Wake, van Dokkum & Franx (2012) using SDSS data.

In Paper XX we used dynamical models to deproject the observed galaxy photometry and stellar kinematics. We demonstrated that velocity dispersion at fixed mass is a direct tracer of the bulge fraction in disc-like galaxies rather than the concentration of a spheroidal distribution, as frequently assumed. This suggests that the presence of a bulge is needed for quenching star formation, in agreement with the photometric study of Bell et al. (2012). However, this does not mean that all these galaxies are undergoing MQ; for instance, the quenching could be due to the presence of an active galactic nucleus (AGN; also correlated with bulge mass).

Only a study of the gas content of quenched galaxies can show if these galaxies are simply extremely gas poor, or instead contain gas but have a low SFR. Using the Arecibo radiotelescope, the atomic gas content of a large sample of low-redshift galaxies has recently been measured by the COLD GASS survey (Schiminovich et al. 2010). Stacking of the H I spectra for these galaxies in bins of fixed stellar mass and colour, Fabello et al. (2011) find that at fixed stellar mass and SFR or colour, ETGs contain a lower mass of atomic gas than LTGs, a result which they claim to be in contradiction with MQ. However, the lack of spatial resolution does not allow Fabello et al. (2011) to determine the actual distribution of this atomic gas. Higher resolution observations show that, in ETGs, the H I is typically found in very extended, low surface density discs (Morganti et al. 2006; Oosterloo et al. 2007, 2010; Paper XIII). In particular, Paper XIII shows that these galaxies lack the $N(\text{H I}) > 10^{21}$ cm^{-2} atomic gas typical of the bright disc of spirals. Such low-density gas would not be expected to form stars, independently of any MQ effect. In addition, only measuring the atomic gas content of the galaxies is not enough to draw a conclusion on quenching, since H I is generally very poorly correlated with star formation (Bigiel et al. 2008).

Molecular gas is much better correlated to SFR, as seen in the comparison of molecular gas mass with Hβ absorption line strength for the ATLAS[3D] sample (Paper IV). The COLD GASS survey (measuring the CO mass for a subsample of the COLD GASS

galaxies) has revealed strong trends between SFR, gas content and morphology (Saintonge et al. 2011a,b, 2012). They find that bulge-dominated galaxies fall into two categories. Some of them have very little cold gas and thus naturally do not form stars. The others contain gas (at surface densities similar to spiral galaxies) but tend to be inefficient at converting it into stars. More exactly, what Saintonge et al. (2011b, 2012) find is a longer molecular gas depletion time-scale (defined as M_{H_2}/SFR) in galaxies with a high stellar mass surface density and a high concentration index, that is, bulge-dominated galaxies. These galaxies are also clearly offset from the Kennicutt relation defined by spirals: the most bulge-dominated galaxies are all found below the mean relation.

6.4 Implications for low and high redshift

In agreement with others, our work shows that for a similar gas content, ETGs form stars less efficiently than LTGs. This does not imply that red ETGs are gas rich: in the local Universe, only 22 per cent of ETGs contain molecular gas, and when gas is present the gas fraction is often much lower than in spirals (Young et al. 2011). This is not in contradiction with MQ, which is simply stating that when gas is present in ETGs it should be more stable against star formation. At high redshift ($z > 1$), galaxies are generally more gas rich, leaving more room for MQ to influence their SFR and colour. Ceverino et al. (2010) indeed found a case of MQ in one of their zoom-in cosmological simulations at $z = 1.3$, with a disc stabilized by the presence of a massive bulge. In their case, the bulge is formed by the coalescence of giant clumps during a phase of violent disc instability: this shows that MQ is an efficient mechanism whatever the origin of massive spheroids.

However, this does not mean that all ETGs should be red and non-star forming. Indeed, only relatively small amounts of gas can be kept stable. As already shown in M09 and again in this paper, gas discs with too high surface densities can fragment, and then form stars with only a slightly lower efficiency than spiral galaxies. Another limitation is that for ETGs with a stable gas disc, interactions with small satellites could be enough to destabilize the disc and trigger some star formation.

As a conclusion, MQ by itself cannot turn all ETGs red, but can definitely help in combination with other mechanisms. It also means that there might not be an absolute need to prevent slow halo gas cooling through AGN feedback (Croton et al. 2006) or gravitational heating (Johansson, Naab & Ostriker 2009). These mechanisms may happen anyway, but in cases where they are inefficient and gas cools from the hot halo, this gas might simply join the disc and be stabilized, allowing the galaxy to remain red.

To test the importance of MQ for the build-up of the red sequence, we use a hydrodynamic simulation of a cosmological volume of $(24 \, h^{-1} \, \text{Mpc})^3$ (Gabor et al. 2011). This simulation captures galaxy accretion and outflows, but cannot resolve morphologies, gas stabilities and SFEs. Producing red galaxies in that simulation required a 'merger quenching' model in which an explicit superwind expels all the gas from the remnant immediately following a major merger. Because of gas reaccretion from the intergalactic medium, the merger remnants still harboured significant levels of star formation and were not red enough. In addition, no colour bimodality was found in the simulation (see Gabor et al. 2011).

We aim to test if an explicit decrease of the SFE in these post-merger galaxies (i.e. imposing MQ in a simulation that is not able to resolve it) could produce more realistic galaxy colours and statistically change the properties of the sample. We select a small sample of 14 galaxies in the cosmological simulation, targeting galaxies

that have at $z = 0$ a stellar mass between 10^{10} and 10^{11} M$_\odot$ and a relatively red colour (an intrinsic[1] $g - r$ greater than 0.45) . We extract their star formation histories and decrease their SFE whenever they have a bulge-dominated morphology. Unfortunately, the resolution of the simulation does not allow us to follow morphological evolution with confidence, so instead we identify ETGs based on their $g - r$ colour. We assume ETGs to have an intrinsic $g - r$ greater than 0.5, which is the end of the blue cloud identified by Gabor et al. in that simulation, and roughly corresponds to galaxies with a specific SFR (defined as the ratio between SFR and stellar mass) lower than 10^{-11} yr^{-1}. The galaxies bluer than 0.5 are unaffected by our SFE reduction scheme: they are assumed to be disc galaxies (some of them might be blue ETGs but not changing their SFE is then a conservative choice). The red galaxies are assumed to be ETGs, and have their SFE reduced by a factor going from 1 (if $g - r = 0.5$) to 4 (if $g - r > 0.65$). 20 per cent of the red galaxies are left unaffected to account for the fact that some of these galaxies could be discs. We also tested three other schemes for reducing the SFE in ETGs, but they all provide consistent results.

As a function of time, as we reduce the SFE in some galaxies, we also modify their gas content self-consistently: a galaxy with a reduced SFE should consume less of its gas, thus providing additional fuel for future star formation. At a given time-step, if we reduce the SFE, we then also increase the gas mass to keep the same total baryonic content as in the initial simulation. At the next time-step, we use this new gas mass to compute a new SFR and $g - r$ (the SFR is computed assuming the Kennicutt relation with the modified SFE). If the galaxy is still red, we continue to apply a SFE correction at the following time-step, possibly by a different amount depending on the $g - r$ colour. Note that we also track stellar mass loss: when the SFR is decreased, less gas is also reinjected into the ISM by stellar mass loss.

We show in Fig. 8 the resulting colour distributions for the original simulation and for the galaxies with a modified SFE, using seven snapshots between $z = 0$ and 0.2 to increase the statistics (although all data points are then not totally independent). The error bars represent the range of values obtained with the four different schemes we tested. As expected, these schemes do not affect much the blue galaxies, but make the red ones significantly redder. In all cases, this creates a bimodal colour distribution. While this does not imply that MQ is the mechanism creating this bimodality in observed galaxies, and while our sample is small, it shows that a decrease by a factor of 2–5 of the SFE in ETGs is enough to have consequences for the reddening of galaxies.

7 CONCLUSIONS

Stability analyses predict that gas discs should be more stable when they are embedded in an ETG instead of a spiral. This increased stability is due in part to the steeper potential well in ETGs, and mostly to the absence of stars contributing to the disc self-gravity. We have previously shown in M09 a cosmological zoom-in simulation in which a gas disc was naturally kept stable in an ETG, forming stars at a low rate, and allowing the galaxy to have red colours in spite of a large gas reservoir.

In this paper, we further study the SFE in ETGs and spirals. Using both the simulation from M09 and a new sample of 5 pc resolution idealized simulations, we confirm that gas discs are significantly more stable in ETGs, and that their SFE is reduced by a factor of
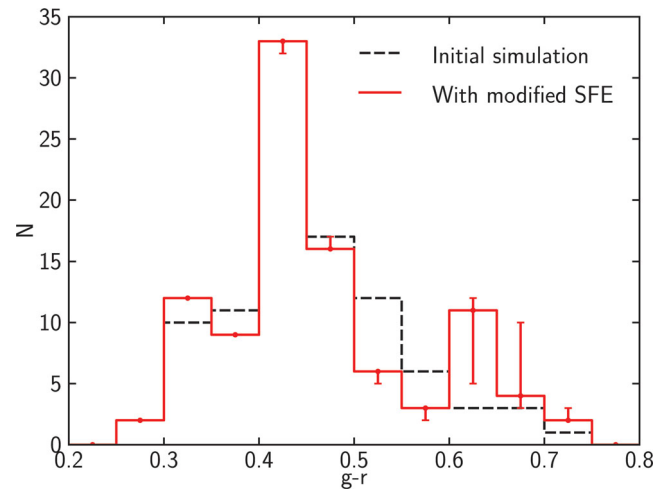
___
[1] There is no dust correction.

Figure 8. Effect of a modified SFE on the $g - r$ colour of simulated galaxies. Following the method described in the text, we artificially reduce the SFE for a sample of simulated ETGs extracted from a cosmological simulation that does not resolve disc stability and MQ. The black dashed line shows the initial distribution of colours, with a lack of red galaxies. The red line shows the colour distribution when the SFE is reduced in ETGs as described in the text (the error bars show the range of values obtained for the different schemes we tested). Reducing the SFE by a factor of a few is enough to significantly redden the galaxies, and to create a red sequence.

2–5. From that small sample of simulations, it also seems that the slope of the Kennicutt relation is steeper for ETGs compared to spirals. This could be due to our star formation recipes, but is found both in the cosmological and in the idealized simulations, which are very different in terms of the technique and resolution used. Instead, it could also be a direct consequence of MQ, with an even increased stability of gas discs at low densities, and at high densities a behaviour getting closer to what is found in spiral galaxies. A larger sample of simulations would be needed to understand that aspect.

We also compare a sample of eight local ETGs to 12 local spirals. For all these galaxies, we use a similar way of measuring CO and H I surface densities, and SFR densities from the non-stellar 8 μm emission. We confirm that the ETGs are slightly offset from the Kennicutt relation defined by the spirals, as also found for the COLD GASS sample by Saintonge et al. (2012). We further validate our approach by performing a direct comparison between models and observations. We run a simulation designed to mimic the stellar and gaseous properties of NGC 524, a local lenticular galaxy, and find a gas disc structure and global SFR in good agreement with the observations.

We thus conclude that, given a similar average gas density, the SFR is a few times lower in ETGs than in LTGs. This lower global efficiency arises in spite of a common universal law for star formation on small scales. The cause is the different structure of the gas in both cases, with in ETGs a lack of gas at high densities. The difference between galaxy types is not only a difference of atomic-to-molecular gas conversion, but also (and most importantly) a difference within the molecular gas itself. Our simulations predict that in a quenched gas disc in an ETG the fraction of dense molecular gas should be much lower than in spirals (with variations as a function of gas content and galaxy morphology). Such a lower fraction of dense molecular gas has tentatively been observed in Paper XI.

ACKNOWLEDGEMENTS

REFERENCES

Agertz O., Teyssier R., Moore B., 2009, MNRAS, 397, L64
Arimoto N., Sofue Y., Tsujimoto T., 1996, PASJ, 48, 275
Bell E. F., 2008, ApJ, 682, 355
Bell E. F. et al., 2012, ApJ, 753, 167
Bigiel F., Leroy A., Walter F., Brinks E., de Blok W. J. G., Madore B., Thornley M. D., 2008, AJ, 136, 2846
Bournaud F., Elmegreen B. G., Teyssier R., Block D. L., Puerari I., 2010, MNRAS, 409, 1088
Bournaud F. et al., 2011, ApJ, 730, 4
Cappellari M., 2002, MNRAS, 333, 400
Cappellari M., 2008, MNRAS, 390, 71
Cappellari M., 2011b, Paper presented at the conference on Galaxy Formation held 2011 July 18–22 at Durham University, Durham, UK (available at: http://astro.dur.ac.uk/Gal2011/talks.php)
Cappellari M. et al., 2007, MNRAS, 379, 418
Cappellari M. et al., 2011, MNRAS, 413, 813 (Paper I)
Cappellari M. et al., 2012a, Nat, 484, 485
Cappellari M. et al., 2013, MNRAS, 432, 1862 (Paper XX)
Ceverino D., Dekel A., Bournaud F., 2010, MNRAS, 440
Cirasuolo M. et al., 2007, MNRAS, 380, 585
Crocker A. F., Bureau M., Young L. M., Combes F., 2008, MNRAS, 386, 1811
Crocker A. F., Jeong H., Komugi S., Combes F., Bureau M., Young L. M., Yi S., 2009, MNRAS, 393, 1255
Crocker A. F., Bureau M., Young L. M., Combes F., 2011, MNRAS, 410, 1197
Crocker A. et al., 2012, MNRAS, 421, 1298 (Paper XI)
Crocker A. et al., 2013, ApJ, 762, 79
Croton D. J. et al., 2006, MNRAS, 365, 11
Daddi E. et al., 2010, ApJ, 714, L118
Dale D. A. et al., 2009, ApJ, 703, 517
Davis T. A. et al., 2011a, MNRAS, 414, 968 (Paper V)
Davis T. A. et al., 2011b, MNRAS, 417, 882 (Paper X)
Davis T. A. et al., 2013, MNRAS, 429, 534
Dekel A., Sari R., Ceverino D., 2009, ApJ, 703, 785
Dubois Y., Teyssier R., 2008, A&A, 477, 79
Emsellem E., Monnet G., Bacon R., 1994, A&A, 285, 723
Fabello S., Catinella B., Giovanelli R., Kauffmann G., Haynes M. P., Heckman T. M., Schiminovich D., 2011, MNRAS, 411, 993
Feldmann R., Gnedin N. Y., Kravtsov A. V., 2012, ApJ, 747, 124
Franx M., van Dokkum P. G., Förster Schreiber N. M., Wuyts S., Labbé I., Toft S., 2008, ApJ, 688, 770
Gabor J. M., Davé R., Oppenheimer B. D., Finlator K., 2011, MNRAS, 417, 2676
Gao Y., Solomon P. M., 2004, ApJ, 606, 271
Genzel R. et al., 2010, MNRAS, 407, 2091
Grand R. J. J., Kawata D., Cropper M., 2012, preprint (arXiv:1209.4083)
Graves G. J., Faber S. M., Schiavon R. P., 2009, ApJ, 698, 1590
Grossi M. et al., 2009, A&A, 498, 407
Gunawardhana M. L. P. et al., 2011, MNRAS, 415, 1647
Helfer T. T., Thornley M. D., Regan M. W., Wong T., Sheth K., Vogel S. N., Blitz L., Bock D. C.-J., 2003, ApJS, 145, 259
Hoversten E. A., Glazebrook K., 2008, ApJ, 675, 163
Johansson P. H., Naab T., Ostriker J. P., 2009, ApJ, 697, L38
Julian W. H., Toomre A., 1966, ApJ, 146, 810
Kaneda H., Onaka T., Sakon I., Kitayama T., Okada Y., Suzuki T., 2008, ApJ, 684, 270
Kauffmann G. et al., 2003, MNRAS, 341, 54
Kawata D., Cen R., Ho L. C., 2007, ApJ, 669, 232
Kennicutt R. C., Jr, 1998a, ARA&A, 36, 189
Kennicutt R. C., Jr, 1998b, ApJ, 498, 541
Kennicutt R. C., Jr et al., 2003, PASP, 115, 928
Krips M., Crocker A. F., Bureau M., Combes F., Young L. M., 2010, MNRAS, 407, 2261
Krumholz M. R., Thompson T. A., 2007, ApJ, 669, 289
Krumholz M. R., Dekel A., McKee C. F., 2012, ApJ, 745, 69
Lablanche P.-Y. et al., 2012, MNRAS, 424, 1495 (Paper XII)
Lada C. J., Forbrich J., Lombardi M., Alves J. F., 2012, ApJ, 745, 190
Martig M., Bournaud F., Teyssier R., Dekel A., 2009, ApJ, 707, 250 (M09)
Meurer G. R. et al., 2009, ApJ, 695, 765
Morganti R. et al., 2006, MNRAS, 371, 157
Narayanan D., Krumholz M. R., Ostriker E. C., Hernquist L., 2012, MNRAS, 421, 3127
Noeske K. G. et al., 2007, ApJ, 660, L43
Oosterloo T. A., Morganti R., Sadler E. M., van der Hulst T., Serra P., 2007, A&A, 465, 787
Oosterloo T. et al., 2010, MNRAS, 409, 500
Ostriker J. P., Peebles P. J. E., 1973, ApJ, 186, 467
Renaud F., Kraljic K., Bournaud F., 2012, ApJ, 760, L16
Saintonge A. et al., 2011a, MNRAS, 415, 32
Saintonge A. et al., 2011b, MNRAS, 415, 61
Saintonge A. et al., 2012, ApJ, 758, 73
Salmi F., Daddi E., Elbaz D., Sargent M. T., Dickinson M., Renzini A., Bethermin M., Le Borgne D., 2012, ApJ, 754, L14
Salucci P., Burkert A., 2000, ApJ, 537, L9
Schiminovich D. et al., 2007, ApJS, 173, 315
Schiminovich D. et al., 2010, MNRAS, 408, 919
Scott N. et al., 2012, preprint (arXiv:1211.4615)
Serra P. et al., 2012, MNRAS, 422, 1835 (Paper XIII)
Shapiro K. L. et al., 2010, MNRAS, 402, 2140
Solomon P. M., Downes D., Radford S. J. E., Barrett J. W., 1997, ApJ, 478, 144

Teyssier R., Chapon D., Bournaud F., 2010, ApJ, 720, L149

Thom C. et al., 2012, ApJ, 758, L41

Tonini C., Maraston C., Thomas D., Devriendt J., Silk J., 2010, MNRAS, 403, 1749

Truelove J. K., Klein R. I., McKee C. F., Holliman J. H., II, Howell L. H., Greenough J. A., 1997, ApJ, 489, L179

van Dokkum P. G., Conroy C., 2010, Nat, 468, 940

Wake D. A., van Dokkum P. G., Franx M., 2012, ApJ, 751, L44

Walter F., Brinks E., de Blok W. J. G., Bigiel F., Kennicutt R. C., Jr, Thornley M. D., Leroy A., 2008, AJ, 136, 2563

Wild W., Harris A. I., Eckart A., Genzel R., Graf U. U., Jackson J. M., Russell A. P. G., Stutzki J., 1992, A&A, 265, 447

Williams R. J., Quadri R. F., Franx M., van Dokkum P., Toft S., Kriek M., Labb I., 2010, ApJ, 713, 738

Wilson C. D., 1995, ApJ, 448, L97

Wu H., Cao C., Hao C.-N., Liu F.-S., Wang J.-L., Xia X.-Y., Deng Z.-G., Young C. K.-S., 2005a, ApJ, 632, L79

Wu J., Evans N. J., II, Gao Y., Solomon P., Shirley Y. L., Vanden Bout P. A., 2005b, ApJ, 635, L173

Wuyts S. et al., 2011, ApJ, 742, 96

Xilouris E. M., Madden S. C., Galliano F., Vigroux L., Sauvage M., 2004, A&A, 416, 41

Young L. M., Bureau M., Cappellari M., 2008, ApJ, 676, 317

Young L. M. et al., 2011, MNRAS, 414, 940 (Paper IV)

Zhu Y.-N., Wu H., Cao C., Li H.-N., 2008, ApJ, 686, 155

This paper has been typeset from a TEX/LATEX file prepared by the author.